Application of extended-crystal diffraction techniques to the symmetry and structure analysis of 221-PbBiSrCaCuO.

P. Goodman,

School of Physics, University of Melbourne, Parkville 3052, Australia

and

P. Miller,

Divison of Materials Science and Technology, CSIRO, Clayton 3168, Australia

ABSTRACT

The discovery of a series of layer-perovskite superconducting compounds by Maeda et al. (1988) presented a challenge for present day electron diffraction techniques,due to their common occurence as mixed phases, and the existence of complex structural modulations of more than one type.

Cowley's (1976) theory developed specifically for describing diffraction effects from layered crystals having a micro-domainal sub-structure seems particularly well suited to the task of solving these structures, while the technique of extended-crystal diffraction as used both in LACBED and SAD is shown here to be capable of providing data of sufficient precision for this analysis.

The present study is made on the 221 compound of PbBiSrCaCuO. Using the above diffraction techniques we show that the true symmetry of the whole structure is orthorhombic, Amaa, and not monoclinic as previously assumed, and that the superlattice reflections arise as a result of a basic microdomainal constitution, rather than from a uniform and incommensurate modulation.

I. Introduction

Convergent beam electron diffraction can now be seen in (at least) three forms. Micro-diffraction, developed in response to the theoretical discoveries of the 1950's [1], can be seen as an extension of Möllenstedt's technique [2] to the back focal microscope objective plane [3]. Later, extended surface diffraction techniques (LACBED) were developed with greatly enhanced information density [4]. Fitting somewhere between these extremes is the more generally applicable materials investigation method whereby bulk materials are thinned, and electron cross-overs of intermediate size (10nm - 100nm) are used [5]. To this list should be added (sub-)nano-meter diffraction [6], [7], which is a direct consequence of high-resolution STEM imaging. These forms are not in any sense competing since the appropriate technique is almost completely determined by the form of the specimen (and with the last-mentioned case also by the budget of the laboratory), as well as by the type of information sought.

Adding interest to this technology, new types of materials are increasingly found to have modulated structures of various sorts which have been discovered and studied both by electron and by single-crystal X-ray diffraction. High on the list of these materials are the Bismuth-based superconducting compounds [8] $Pb_xBi_{2-x}Sr_2Ca_{n-1}O_y$, where 'x' ranges from 0 to ≅ 0.3, which form a well-known series for $1 < n < 3$, although compounds may be formed to at least $n = 5$. Needless to say, these compounds have attracted a lot of attention; so much so that within a year of their discovery possibly over 50 separate studies appeared detailing their crystallography and superlattice modulation. Nevertheless some of the basic questions relating to the microstructure of these compounds remain unsolved, with much of the evidence in conflict.

The $n = 1$ and $n = 2$ structures have been the most studied and are in a sense the most interesting; they are contrasted in that the $n = 1$ structure has only a single 'strontium-type' layer in which to accommodate the mixture of Sr and Ca usually incoroprated, and so takes on some solid-solution character.

From the start one of the points in dispute has been the

so-called 'average' symmetry, with an equal number of studies finding the centric and non-centric space groups Amaa and A2aa. At first we thought this was probably a consequence of the symmetry depending upon precise composition and details of preparation. With the acccumulation of evidence this no longer seems a satisfactory situation. Nor does the present level of understanding of the relationship between the cuperlattice and the average or sublattice structure.

However the theoretical formulation which would allow this understanding is already in place, in the form of Cowley's general treatment of structures with irregular compositional faults [9]. If this were to be implemented in a quantitative way in the present 3-dimensional problem, no doubt more extensive data than the present meagre set would be required. Although this has not yet been done, we feel we have taken a step in the right direction by presenting here sufficient evidence to at least show that this is the right way to go.

Since symmetry determination for the sub-cell requires LACBED patterns while that for the supercell requires focussed SAD patterns we present this data in two sections. The compound we investigate here is the Sr-poor version of the 221 structure, since this has been the subject of the most detailed X-ray single crystal analysis available to us [10].

2.1 CBED and LACBED examination of the PbBiSrCaCuO series.

Fig.1 shows idealised atomic models for the n = 1,2,3 structures of the series.

ZOLZ CBED pattern for the compounds n = 1,2,3 and 5 are shown in Fig.2. From these patterns it is seen that only the n = 1 compound displays the double mirror symmetry of Amaa; in the case of the n = 3 and 5 compounds the visiblity of the first and higher-order Laue-zone lines clearly shows the break of symmetry across b*. This higher symmetry for n = 1 may be thought of as a consequence of the Sr-Ca solid-solution character mentioned above.

The n = 1 composition used for this series was determined by EDX to follow the formula $Pb_{0.2}Bi_{1.8}Sr_{1.7}Ca_{0.3}CuO_y$, where the Cu content was not measured since a Cu supporting grid was used. This

Pb-Bi and Sr-Ca layers. Since the analysis by Gao et al. [10] was made for a Sr-poor/Bi-rich sample, a second preparation was made which gave the formula $Pb_{0.2}Bi_{1.8}Sr_{1.3}Ca_{0.25}CuO_y$ with EDX analysis. This preparation also gave extensive micaceous sheets, so that a specimen could be prepared by glueing a crystal onto a 100 mesh Cu grid and stripping it from above with sticky tape until an electron transparant film was formed.

Fig.3 shows the set of dark-field LACBED patterns surrounding a central bright-field pattern, obtained for this sample. This set of patterns shows more convincingly than any single CBED pattern that the structure is centric, and that the space group is still Amaa. Apart from the two whole-pattern mirror planes evident from the reflection symmetry between the 220 and 2 -2 0 patterns, and across the 020 pattern, the presence of the third mirror plane is evidenced by the centro-symmetry of all and particularly of the 2 ±2 0 patterns; the presence of the two horizontal diads, missing from space group A2aa, is seen from the internal mirror lines within the 200 and 020 patterns.

Apart from these patterns, Fig.4 shows the CBED pattern taken from the same area of film. In this case we see an indecisive result, which has arisen due to a combination of local beam damage and natural film curvature which frequently occurs with a soft material. This kind of effect has been responsible for much of the uncertainty of results so far by CBED from this material.

2.2 Alchemi analysis.

ALCHEMI [11] analysis was attempted using the extended natural (001) face, which permits the use either of a defocused beam, or constant shifting of the beam focus, in order to reduce beam damage.

Ultimately 45 spectra were recorded, with a 300kV focussed beam. Channelling conditions were varied by using the beam-tilt controls, and the crystal was cooled to about 100K using a Gatan low-background double-tilt cold stage. With a convergence angle of 0.9 mrad significant channelling effects were recorded.

Typical peak intensities were about 4000 counts for Pb Lα, 3600 counts for Ca Kα, 22,000 for Sr Kα and 36,000 counts for Bi Lα.

Finally, the distribution of Pb over 3 (Bi, Sr, and Ca) sites in the $Pb_{0.2}Bi_{1.8}Sr_{1.3}Ca_{0.25}Cu_1O_y$ structure was:

Ca (0.174) Pb (0.076 ± 0.028)
Bi (1.995) Pb (0.006 ± 0.032)
Sr (1.312) Pb (0.098 ± 0.037)

where the uncertainties represent one standard deviation. At the conclusion of this experiment it was realised that even better results would have been obtained if the illumination conditions of LACBED (with a beam irradiation area ≅ 10 nm) had been adhered to. Nevertheless these results do give the significant indication that the Pb atoms are substituting for Ca rather than Bi with this composition. Since the formula $Pb_{0.2}Bi_{1.8}Sr_{1.3}Ca_{0.25}CuO_y$ would fit as $(Bi)_{1.8}(SrCaPb)_{1.75}CuO$, normalising again to $Bi_2(SrCaPb)_2CuO$, it appears that the ALCHEMI result also makes structural sense. It is interesting to note that the X-ray single crystal study for this compound found Bi substituting for Sr [10]; however in the X-ray study, unlike the EDX study, it was not possible to distinguish Pb and Bi.

3.1 Superlattice Observation.

First, we look at results from a previous analysis of the n = 2 structure [12]. Fig.5(a) shows the selected-area (SAD) pattern taken for this $Bi_2Sr_2CaCu_2O_y$ (Pb-free, x = 0) structure, for which the superlattice is seen to run in segments inclined at a small angle to the main reciprocal lattice rows. The value of this angle is dependent upon the oxidation state of the compound, and can be zero. An enlargement showing this effect is seen in Fig. 5(b). This characteristic suggests that a crystallographic or Wadsley-type shear mechanism is present and that the superlattice is the result of a possibly commensurate micro-domainal structure. A prediction of this type from diffraction pattern analysis [12] appears to have been confirmed by direct lattice images [13]. In any case the symmetry consequences of this shear angle are clear: the mirror symmetry of Amaa is broken by the superlattice. Furthermore, the micro-domainal interpretation runs counter to the commonly used interpretation in terms of a continuous but incommensurate modulation vector.

We now return to the 221 structure which we are currently

investigating and for which we have much more accurate SAD data. The reason for this increased accuracy is that we have here for the first time used the same extended area for the SAD as was used for the LACBED patterns of Fig.3. This means that the crystal has been very accurately aligned to the [001] direction. Fig. 6 (a) shows the low-magnification view of the zone-axis pattern. From this two features are apparant. One is the diffuse streaks, parallel to {110}, which run both radially and circumferentially through the pattern. The second is the fact that the superlattice spacings are decidedly irregular, as seen in the enlargement of Fig.6 (b). In fact, the region where the most extensive run of superlattice spots occurs is around the intersection of the radial and transverse diffuse bands, in the FOLZ region, where runs of 3 or 4 spots occur which have an almost exact 7-fold lattice spacing. If one section of the FOLZ pattern is examined in isolation it appears precisely as if these 7-fold lattice rows run at an inclination to [001] and so are only intercepted in segments, but in contrast to the n = 2 structure (Fig.5) there is no apparent inclination to the a* axis.

However when the pattern is taken as a whole it is seen that the Amaa symmetry is <u>not</u> broken, and that details of the aperiodicity observed in the superlattice spacings and intensities are accurately reflected across both a* and b* axes. This is seen in Fig.7, where two strips of pattern, parallel to a* and b* are shown enlarged.

3.2 Superlattice Interpretation.

Several consequences of the above observations emerge. One is that the overall symmetry is still centric and orthorhombic, and not monoclinic as previously stated in several publications, although a monoclinic interpretation is readily understandable. Our interpretation is in fact that the high symmetry is the result of averaging over lower-symmetry micro-domains, the presence of domain walls being deduced from the diffuse bands. It would also appear that these low-symmetry domains are of shallow depth and contain a 7-fold modulation with an individual sub-lattice origin. This interpretation, illustrated schematically in Fig.8, would account for the more complete superlattice presence in the FOLZ region, as compared with the central ZOLZ region in which a

projection of the structure would see destructive interference of superlatice spots between domains.

4. Conclusions.

A question which may often be asked about extended perfect crystals is, how can the information derived by EM examination be increased in proportion to the usable area? In diffraction experiments, using more parallel illumination obviously reduces radiation damage and this contributes to a better quality of pattern. Then, the LACBED technique offers an enormously increased information density in diffraction patterns. However what has perhaps not been appreciated before is that it also offers a similar increase in accuracy to the SA-focussed diffraction pattern. The symmetry observed in Figs.6 and 7 is the result of having the incident beam not only parallel to the zone axis, but normal to the crystal surface which determines the direction of the reciprocal lattice spikes.

The observations presented show that the overall symmetry of the 221 phase is orthorhombic as a result of averaging over microdomains. Consequently it seems that in this case the application of supergroup theory [14] would be inappropriate, and counterproductive in terms of arriving at a real space solution. On the other hand, Cowley's theory which was developed specifically to treat micro-domainal structures could readily be adapted to this problem. Grzdinic [15] has in fact made an extension of this theory to perovskite-based structures, and plots from his calculations for $K_{x.54}Mg_{0.77}Ti_{7.23}O_{16}$ give results surprisingly similar in character to observations of superlattice spots neighbouring Bragg positions in our patterns.

Following these observations, further quantitative work on this analysis is planned.

REPLACE

Acknowledgements.

We firstly wish to thank Shaun Bulcock for supplying single crystals from his research project for our examination.

This work has been supported by the Australian Research Council through their grant No. A68930390.

The observations presented show that the overall symmetry of the 221 phase is orthorhombic, although segments of the pattern show a marked irregularity of spacing. The high symmetry is interpreted as arising from an averaging over microdomains, while the irregularity is symptomatic of

FIGURE CAPTIONS

Fig.1 Atomic arrangements in idealised models of the n = 1, 2 and 3 structures of the compound $(PbBi)_2Sr_2Ca_{n-1}Cu_nO_y$.

Fig.2. ZOLZ CBED patterns for the n = 1, 2, 3 and 5 memebers of the structural series $(PbBi)_2Sr_2Ca_{n-1}Cu_nO_y$.

Fig.3. Set of dark-field patterns from $Pb_{0.2}Bi_{1.8}Sr_{1.3}Ca_{0.25}Cu_1O_y$ surrounding the bright-field LACBED pattern. The patterns index from left to right (starting on the top row): 220, 200, -2 2 0, 020, 000 (a -> d) and (e) the pair of -2 2 0 and inverted 220 patterns given to show their near identity of features.

Fig.4. Convenentional micro-focus CBED pattern from the same region as used for the LACBED patterns of Fig.3.

Fig.5. [001] zone axis SAD pattern from the n = 2 structure showing the segmentation of the superlattice rows, with an inclination to the b* axis. (a) shows the general pattern; (b) gives an enlargement of detail.

Fig.6. [001] zone axis SAD pattern from $Pb_{0.2}Bi_{1.8}Sr_{1.3}Ca_{0.25}CuO_y$ showing (a) general pattern including diffuse bands;
(b) enlargement of portion of the pattern parallel to a* showing the segments of 7-fold superlattice, marked as a,b,c,d,e, and the overall symmetry of these segments across a central mirror line.

Fig.7. Two strips of pattern enlarged from the pattern of Fig.6(a) which run (a) parallel to a* and (b) parallel to b*, showing the two mirror symmetries.

Fig.8. Schematic illustration of the diffuse {110} bands seen in Fig.6(a), and the interpretation of the superlattice in terms of shallow microdomains carrying the 7-fold modulation with individual phases.

ATOMIC MODELS OF BiSrCaCuO STRUCTURES

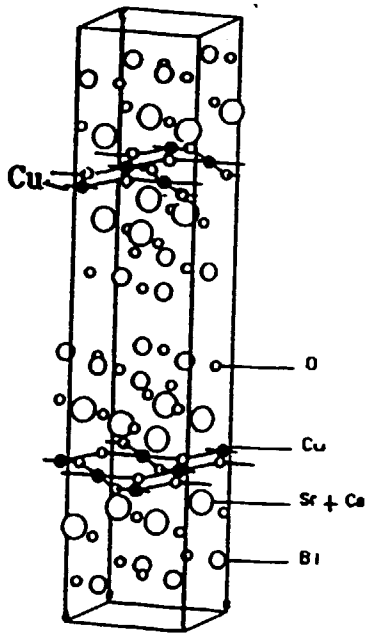

n = 1

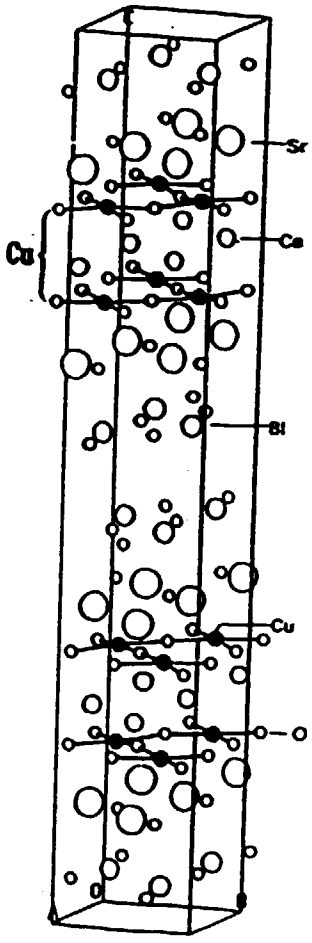

n = 2

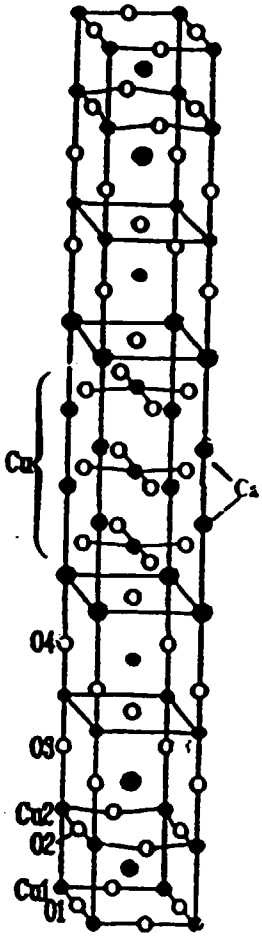

n = 3

Fig 1

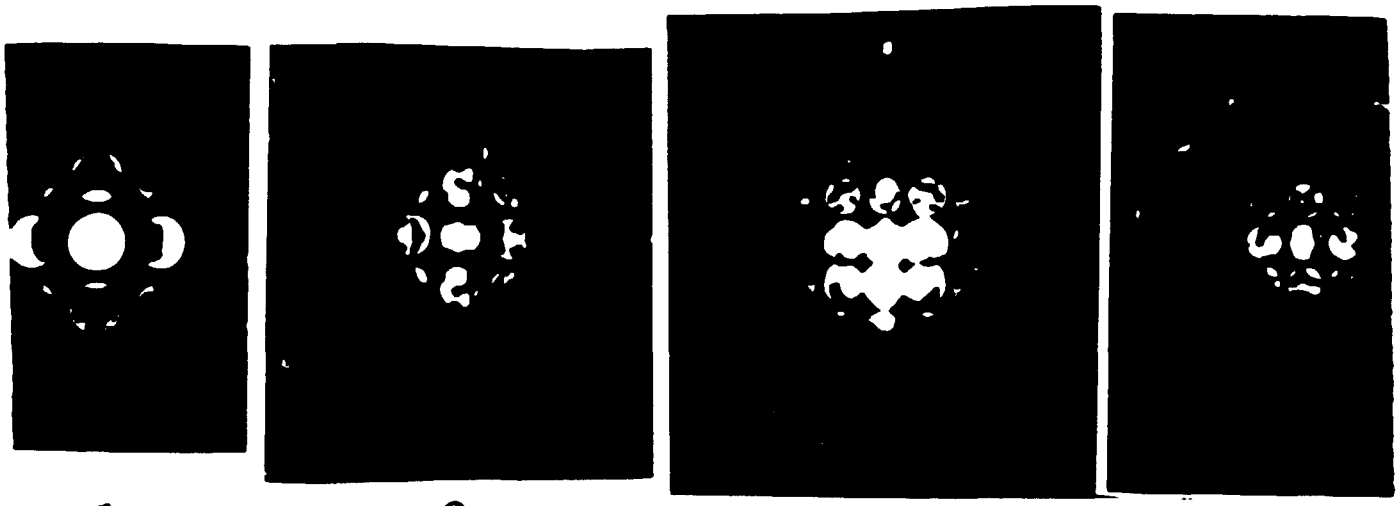

Fig 2.

T-183

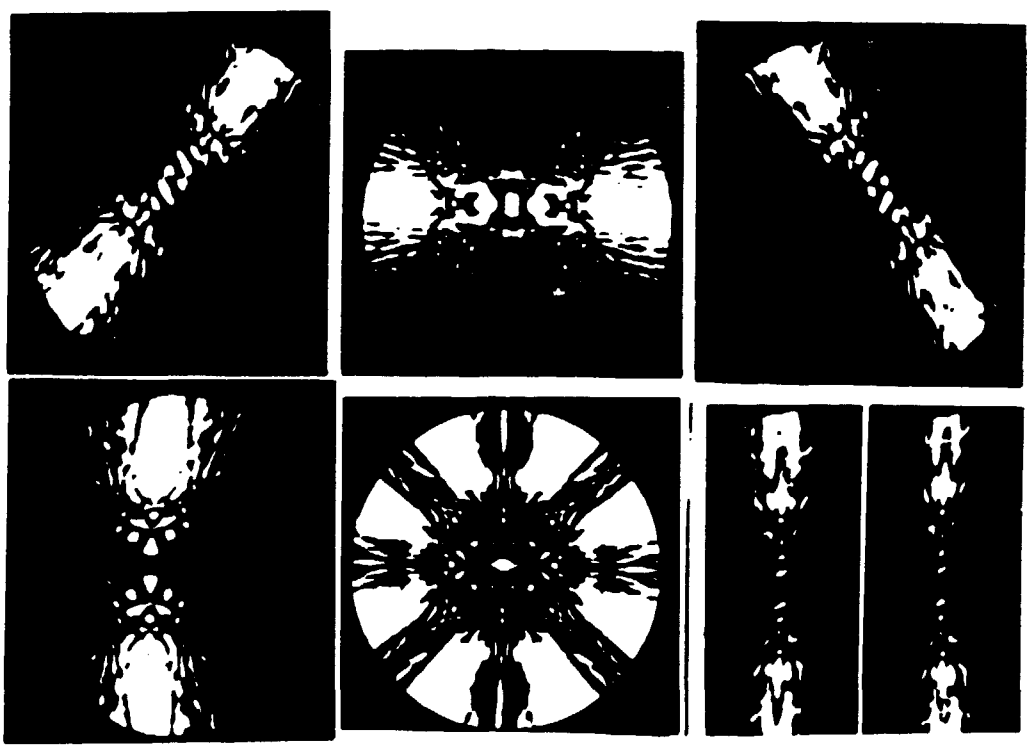

Fig 6

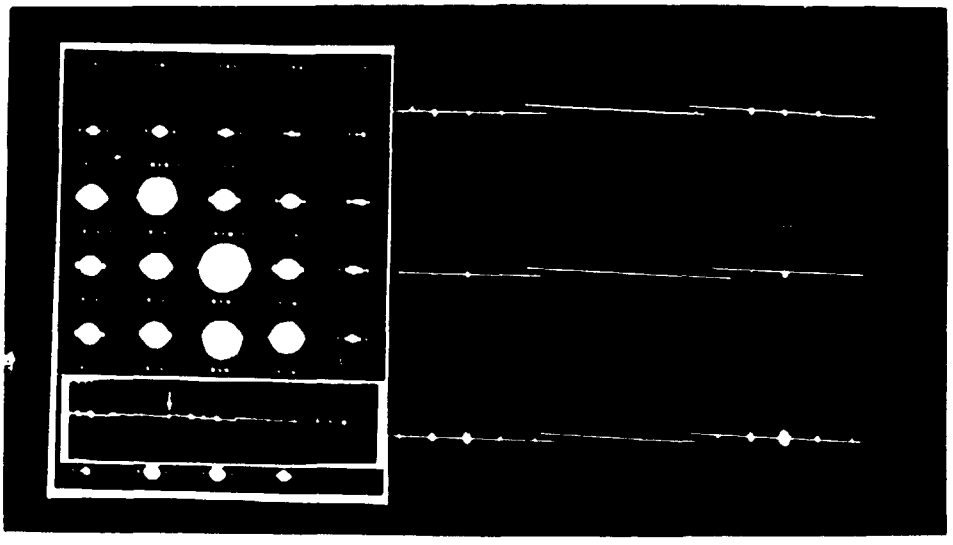

Fig 7

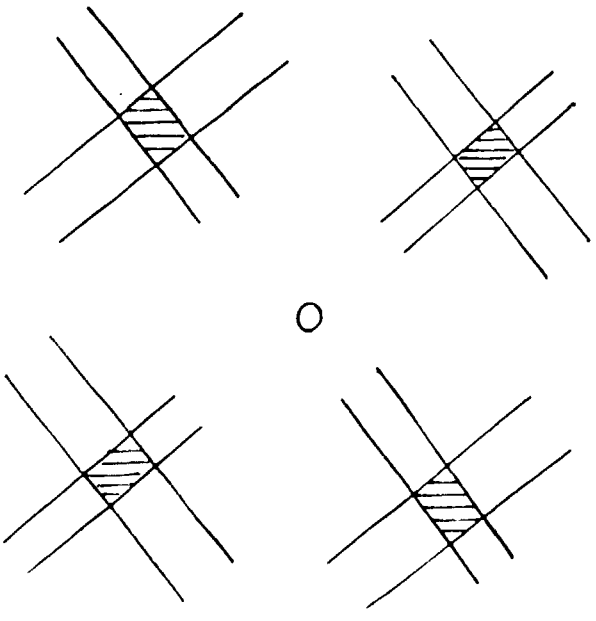

Fig 8